Collision Cones for Quadric Surfaces in n-Dimensions

Animesh Chakravarthy and Debasish Ghose

***Abstract*—In this letter, we present analytical expressions for collision cones associated with a class of hyperquadric surfaces moving in n-dimensional configuration space. Using a relative velocity paradigm, a geometric analysis of the distance, time, and point of closest approach between moving objects in n-dimensional space, is carried out to obtain a characterization of the collision cone between a point and a hyperspheroid as well as a constrained hyperboloid, which represent an interesting and useful class of objects in configuration space. It is shown that these n-dimensional collision cones can be integrated with sampling-based motion planners, avoiding the need to evaluate waypoints that lie inside the collision cone. The cones can also consist of the heading angles toward desirable regions in the configuration space, in which case planners may evaluate more waypoints inside the cone. Finally, analytical expressions of the collision cones are used, in conjunction with the concept of level sets, and incorporated into a Lyapunov-based design approach, to determine analytical expressions of nonlinear guidance laws that can manipulate the velocity vector of an object in n-dimensional space.**

***Index Terms*—Collision avoidance, motion and path planning, collision cones, *n*-dimensions, configuration space.**

I. Introduction

PATH planning in n-dimensional spaces is a problem that has attracted much interest [1]–[4]. In general, these spaces can contain both stationary and moving obstacles. Many sampling based planners such as Probabilistic Road Maps (PRMs) [3] and Rapidly-exploring Random Trees (RRTs) [4] explore regions of this n-dimensional space and look for potential collisions with obstacles. It would be immensely helpful if we could characterize collision-free regions within this space because the sampling based planners then need to explore only these regions [1]. Such a characterization of the collision-free spaces for ellipsoidal bodies with ellipsoidal obstacles is given in [1], which relies on the Minkowski sum and difference of two ellipsoids which have been characterized in [5], [6].

In this letter, we perform an alternative characterization of the collision free regions, by using the notion of collision cones [7]. A collision cone provides the set of heading directions that would cause an object A to be on a collision course with a moving object B. With knowledge of these cones, the sampling planner can then evaluate waypoint samples that lie outside these cones. See Fig. 1 for an illustration, where A represents a point object having to navigate through an n-dimensional configuration space with multiple moving obstacles B_1, B_2, $B_3, \ldots,$ moving with velocities $V_{B1}, V_{B2}, V_{B3}, \ldots$. The collision cones from A to each of these obstacles are represented as $C_1, C_2, C_3,$ ..., and can represent forbidden zones which the sampler either need not evaluate at all, or alternatively, evaluate only with a low probability.

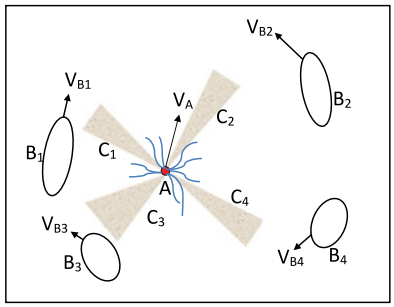

Fig. 1. An object A navigating through an n-dimensional configuration space cluttered with moving obstacles $B_1, B_2, \ldots$ modeled by hyperquadrics.

In cluttered environments where the objects are moving in close proximity, the shapes of the objects play an important role in the determination of collision avoidance maneuvers. In this letter, we provide analytical characterizations of the collision cone when the object B belongs to a class of hyperquadric surfaces [8] which can serve as efficient bounding volumes for a large class of objects. Hyperquadric surfaces include hyperspheres, hyperspheroids, hyperellipsoids, etc. While hyperspheres can be used to bound many object shapes because of the analytical convenience they provide, they can often be conservative when the objects are more elongated in some directions than in other directions. In such scenarios, hyperspheroids serve as better approximations than spheres because they can form a tighter bounding volume on elongated objects. Hyperquadrics such as n-dimensional hyperboloids can be used as bounding volumes for non-convex objects. Objects may also be represented as a union of hyperspheroids and n-dimensional hyperboloids.

Hyperspheroids are also of interest in RRT problems for another reason. In RRT methods, it has been shown that for problems that seek to minimize path length, the subset of states that can improve a solution can be described by a prolate hyperspheroid, whose focal points are the start and goal points [9]. In such problems, the hyperspheroid is not an entity that needs

Manuscript received September 10, 2017; accepted November 1, 2017. Date of publication November 22, 2017; date of current version December 11, 2017. This letter was recommended for publication by Associate Editor E. Johnson and Editor J. Roberts upon evaluation of the reviewers' comments. This work was supported by the National Science Foundation under Grants IIS-1351677 and CNS-1446557. The work of A. Chakravarthy was supported by the National Science Foundation. *(Corresponding author: Animesh Chakravarthy)*

A. Chakravarthy is with the Department of Aerospace Engineering and the Department of Electrical Engineering and Computer Science, Wichita State University, Wichita, KS 67260 USA (e-mail: animesh.chakravarthy@wichita.edu).

D. Ghose is with the Department of Aerospace Engineering, Indian Institute of Science, Bengaluru, Bengaluru 560012, India (e-mail: dghose@aero.iisc.ernet.in).

Digital Object Identifier 10.1109/LRA.2017.2776347

to be avoided, but instead is a region within which the trajectories need to lie, since the optimal path is contained inside the hyperspheroid. Informed RRT* [9] focuses the search on this informed subset of the state space that contains all the states that can improve the current solution. In such problems, we would like to determine the cone of heading angles that lead into the hyperspheroid, so that the sample-based planner then samples only the waypoints that lie within this cone.

This letter determines analytical expressions for collision cones in high-dimensional spaces. The collision conditions for a large class of object shapes moving in 2-D [7] and 3-D [10] has been proposed in the literature. Exact collision conditions for objects of entirely arbitrary shapes (convex and non-convex) in 2-D have been determined in [7], while the same has been determined for objects modeled by quadric surfaces in 3-D in [10]. These conditions have been used to determine analytical expressions of guidance laws for collision avoidance in [11], and for safe-passage through narrow, moving orifices in [12]. At its most fundamental level, the collision cone has some connections with the maneuvering board approach [13], velocity obstacles [14], and forbidden regions [15] in that these approaches determine cones of forbidden heading directions or velocities that cause collisions. However, while all these letters model the objects as circles or spheres, the collision cone approach can handle a larger class of object shapes.

In this letter, we determine collision cones associated with a class of moving hyperquadric surfaces in n-dimensions. The rest of this letter is organized as follows. Section II discusses the collision dynamics between a pair of point objects moving in n-dimensional space. Sections III and IV present the collision cone between a point object and a hyperspheroid, and that between a point object and a hyperboloid, in n-dimensional space. Section V illustrates the collision cone equations with examples, while Section VI illustrates how one can determine analytical guidance laws to facilitate either avoidance of collision between two objects, or rendezvous of the objects. Section VII presents the conclusions.

II. Relative Velocity Kinematics Between Two Point Objects in R^n

Consider two point objects A and B moving in R^n. Let the origin of R^n be at A. In this frame, the co-ordinates of B are expressed as $[\,x_1\ x_2\ \ldots\ x_n\,]$. They can be equivalently expressed in terms of hyperspherical coordinates $(r, \phi_1, \phi_2, ..., \phi_{n-1})$, where r is the distance AB, and $\phi_1, \phi_2, ..., \phi_{n-1}$ are the bearing angles of B with respect to A. The two coordinate systems are related as follows [16], [17]:

$$\begin{aligned}
x_1 &= r\cos\phi_1 \\
x_2 &= r\sin\phi_1\cos\phi_2 \\
x_3 &= r\sin\phi_1\sin\phi_2\cos\phi_3 \\
&\vdots\ \vdots \\
x_{n-1} &= r\sin\phi_1\sin\phi_2\ldots\sin\phi_{n-2}\cos\phi_{n-1} \\
x_n &= r\sin\phi_1\sin\phi_2\ldots\sin\phi_{n-2}\sin\phi_{n-1}
\end{aligned} \tag{1}$$

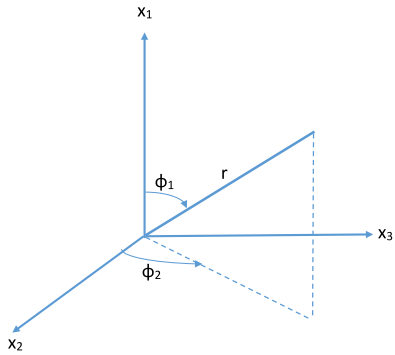

Fig. 2. Schematic showing definition of angles in a 3-D case.

The above equations are illustrated for a 3-D coordinate system in Fig. 2. Let the velocities of A and B be $\vec{V}_A$ and $\vec{V}_B$, respectively. These velocity vectors, $[\,V_{A,x1}\ V_{A,x2}\ ...\ V_{A,xn}\,]^T$, and $[\,V_{B,x1}\ V_{B,x2}\ ...\ V_{B,xn}\,]^T$ have their equivalent representation in spherical co-ordinates as follows:

$$\vec{V}_A = \begin{bmatrix} V_A\cos\alpha_1 \\ V_A\sin\alpha_1\cos\alpha_2 \\ \vdots \\ V_A\sin\alpha_1\sin\alpha_2\ldots\sin\alpha_{n-2}\cos\alpha_{n-1} \\ V_A\sin\alpha_1\sin\alpha_2\ldots\sin\alpha_{n-2}\sin\alpha_{n-1} \end{bmatrix},$$

$$\vec{V}_B = \begin{bmatrix} V_B\cos\beta_1 \\ V_B\sin\beta_1\cos\beta_2 \\ \vdots \\ V_B\sin\beta_1\sin\beta_2\ldots\sin\beta_{n-2}\cos\beta_{n-1} \\ V_B\sin\beta_1\sin\beta_2\ldots\sin\beta_{n-2}\sin\beta_{n-1} \end{bmatrix} \tag{2}$$

where, V_A and V_B are the speeds of A and B, and $(\alpha_1, \alpha_2, ..., \alpha_n)$ and $(\beta_1, \beta_2, ..., \beta_n)$ are the heading angles of $\vec{V}_A$ and $\vec{V}_B$. Define $\vec{V}_{REL} = \vec{V}_B - \vec{V}_A$ as the relative velocity of B with respect to A. Let $\hat{\epsilon}_r$ represent the unit vector along the line AB, and $\hat{\epsilon}_{\phi 1}$, $\hat{\epsilon}_{\phi 2}$, ..., $\hat{\epsilon}_{\phi n-1}$ represent $n-1$ mutually orthogonal unit vectors that are also orthogonal to AB. These unit vectors can be obtained as follows. From (1), we see that the vector $\vec{r}$ is represented as:

$$\vec{r} = r\begin{bmatrix} \cos\phi_1 \\ \sin\phi_1\cos\phi_2 \\ \vdots \\ \sin\phi_1\sin\phi_2\ldots\sin\phi_{n-2}\cos\phi_{n-1} \\ \sin\phi_1\sin\phi_2\ldots\sin\phi_{n-2}\sin\phi_{n-1} \end{bmatrix} \tag{3}$$

From the above, we can find the unit vectors using the equations $\hat{\epsilon}_r = \frac{d\vec{r}}{dr}/|\frac{d\vec{r}}{dr}|$, $\hat{\epsilon}_{\phi 1} = \frac{d\vec{r}}{d\phi_1}/|\frac{d\vec{r}}{d\phi_1}|$, $\hat{\epsilon}_{\phi 2} = \frac{d\vec{r}}{d\phi_2}/|\frac{d\vec{r}}{d\phi_2}|$, ..., $\hat{\epsilon}_{\phi_{n-1}} = \frac{d\vec{r}}{d\phi_{n-1}}/|\frac{d\vec{r}}{d\phi_{n-1}}|$. Since (3) has the form $\vec{r} = r\hat{\epsilon}_r$, the expression for $\hat{\epsilon}_r$ is readily evident, while those corresponding to the other

unit vectors are as follows:

$$\hat{\epsilon}_{\phi 1} = \begin{bmatrix} -\sin\phi_1 \\ \cos\phi_1 \cos\phi_2 \\ \cos\phi_1 \cos\phi_3 \sin\phi_2 \\ \vdots \\ \cos\phi_1 \sin\phi_2 \ldots \sin\phi_{n-2} \cos\phi_{n-1} \\ \cos\phi_1 \sin\phi_2 \ldots \sin\phi_{n-2} \sin\phi_{n-1} \end{bmatrix}$$

$$\hat{\epsilon}_{\phi 2} = \begin{bmatrix} 0 \\ -\sin\phi_2 \\ \cos\phi_2 \cos\phi_3 \\ \vdots \\ \cos\phi_2 \ldots \sin\phi_{n-2} \cos\phi_{n-1} \\ \cos\phi_2 \ldots \sin\phi_{n-2} \sin\phi_{n-1} \end{bmatrix},$$

$$\hat{\epsilon}_{\phi 3} = \begin{bmatrix} 0 \\ 0 \\ -\sin\phi_3 \\ \vdots \\ \cos\phi_3 \ldots \sin\phi_{n-2} \cos\phi_{n-1} \\ \cos\phi_3 \ldots \sin\phi_{n-2} \sin\phi_{n-1} \end{bmatrix},$$

$$\hat{\epsilon}_{\phi n-1} = \begin{bmatrix} 0 \\ 0 \\ 0 \\ \vdots \\ -\sin\phi_{n-1} \\ \cos\phi_{n-1} \end{bmatrix} \tag{4}$$

Differentiating (3), it can be shown that:

$$\begin{aligned} \dot{\vec{r}} = \dot{r}\hat{\epsilon}_r + r\dot{\phi}_1\hat{\epsilon}_{\phi 1} + r\sin\phi_1\dot{\phi}_2\hat{\epsilon}_{\phi 2} \\ + r\sin\phi_1\sin\phi_2\dot{\phi}_3\hat{\epsilon}_{\phi 3} + \ldots \\ + r\sin\phi_1\sin\phi_2\ldots\sin\phi_{n-2}\dot{\phi}_{n-1}\epsilon_{\phi n-1} \end{aligned} \tag{5}$$

We next resolve $\vec{V}_{REL}$ into its n components $V_r, V_{\phi 1}, V_{\phi 2}, \ldots, V_{\phi_{n-1}}$, where V_r represents the relative velocity component along AB and $V_{\phi i}, i = 1, 2, ..., n-1$ are the relative velocity components orthogonal to AB. These relative velocity components are as follows:

$$\begin{aligned} V_r &\equiv \vec{V}_{REL}.\hat{\epsilon}_r = \dot{r} \\ V_{\phi 1} &\equiv \vec{V}_{REL}.\hat{\epsilon}_{\phi 1} = r\dot{\phi}_1 \\ V_{\phi 2} &\equiv \vec{V}_{REL}.\hat{\epsilon}_{\phi 2} = r\sin\phi_1\dot{\phi}_2 \\ &\vdots \\ V_{\phi n-1} &\equiv \vec{V}_{REL}.\hat{\epsilon}_{\phi n-1} = r\sin\phi_1\sin\phi_2\ldots\sin\phi_{n-2}\dot{\phi}_{n-1} \end{aligned} \tag{6}$$

After substituting (3)–(4) in (6), differentiating the resulting expressions, and re-arranging the algebraic terms, we obtain the n differential equations governing the quantities $\dot{V}_r$, $\dot{V}_{\phi 1}$, $\dot{V}_{\phi 2}, \ldots,$ $\dot{V}_{\phi n-1}$. We initially assume that both A and B move with constant velocities (this assumption is relaxed in Section VI). The differential equation governing $\dot{V}_r$ is as follows:

$$r\dot{V}_r = V_{\phi 1}^2 + V_{\phi 2}^2 + \ldots + V_{\phi n-1}^2 \tag{7}$$

The differential equations governing $\dot{V}_{\phi 1}$, $\dot{V}_{\phi 2}$, …, $\dot{V}_{\phi n-1}$ are fairly lengthy, and not presented here due to space considerations. However, as an illustration, the equations for a 4-dimensional scenario, involving the components $\dot{V}_{\phi 1}, \dot{V}_{\phi 2}, \dot{V}_{\phi 3}$ are given in the Appendix.

From the differential equations for the relative velocity components, (8) and (10) presented below, can be determined. (See the Appendix for an illustration of how these equations are determined in a 4-D case). The relative velocity components satisfy the following equation:

$$\dot{V}_r V_r + \dot{V}_{\phi 1} V_{\phi 1} + \dot{V}_{\phi 2} V_{\phi 2} + \ldots + \dot{V}_{\phi n-1} V_{\phi n-1} = 0 \tag{8}$$

which can be integrated to yield:

$$V_r^2 + V_{\phi 1}^2 + \ldots + V_{\phi n-1}^2 = V_r(0)^2 + V_{\phi 1}(0)^2 + \ldots + V_{\phi n-1}(0)^2 \tag{9}$$

where, $V_r(0), V_{\phi 1}(0), V_{\phi 2}(0), ..., V_{\phi n-1}(0)$ are the initial values of the corresponding quantities.

Furthermore, it can be shown that:

$$\frac{\dot{V}_{\phi 1} V_{\phi 1} + \dot{V}_{\phi 2} V_{\phi 2} + \ldots + \dot{V}_{\phi n-1} V_{\phi n-1}}{V_{\phi 1}^2 + V_{\phi 2}^2 + \ldots + V_{\phi n-1}^2} = \frac{-V_r}{r} \tag{10}$$

Integrating both sides of (10) with respect to time, we obtain:

$$\frac{V_{\phi 1}^2 + V_{\phi 2}^2 + \ldots + V_{\phi n-1}^2}{V_{\phi 1}(0)^2 + V_{\phi 2}(0)^2 + \ldots + V_{\phi n-1}(0)^2} = \frac{r(0)^2}{r^2} \tag{11}$$

Let r_m represent the distance between A and B at the instant of closest approach, and let this closest approach occur at time $t = t_m$. Since $V_r = \dot{r}$, we therefore have $V_r(t_m) = 0$. When evaluated at $t = t_m$, (11) thus becomes:

$$\frac{V_{\phi 1m}^2 + V_{\phi 2m}^2 + \ldots + V_{\phi n-1m}^2}{V_{\phi 1}(0)^2 + V_{\phi 2}(0)^2 + V_{\phi 3}(0)^2} = \frac{r(0)^2}{r_m^2} \tag{12}$$

where, $V_{\phi im} = V_{\phi i}(t_m), i = 1, \ldots, n$. Evaluating (9) at $t = t_m$, and substituting $V_{rm} = 0$ in (9), we obtain:

$$V_{\phi 1m}^2 + \ldots + V_{\phi n-1m}^2 = V_r(0)^2 + V_{\phi 1}(0)^2 + \ldots + V_{\phi n-1}(0)^2 \tag{13}$$

From (12) and (13), we obtain the miss-distance as:

$$r_m^2 = \frac{r(0)^2(V_{\phi 1}(0)^2 + V_{\phi 2}(0)^2 + \ldots + V_{\phi n-1}(0)^2)}{V_r(0)^2 + V_{\phi 1}(0)^2 + V_{\phi 2}(0)^2 + \ldots + V_{\phi n-1}(0)^2} \tag{14}$$

The objects A and B are at a distance r_m apart, at the miss time t_m, which represents the time instant at which A and B achieve their closest approach, and is given by:

$$t_m = \frac{-r(0)V_r(0)}{V_r(0)^2 + V_{\phi 1}(0)^2 + V_{\phi 2}(0)^2 + \ldots + V_{\phi n-1}(0)^2} \tag{15}$$

Note that in the above equation, t_m is positive only when $V_r(0)$ is negative. If the initial conditions are such that $V_r(0)$ is positive, then t_m is negative and corresponds to the time at which closest approach would occur if the trajectories of both A and B were projected backwards in time.

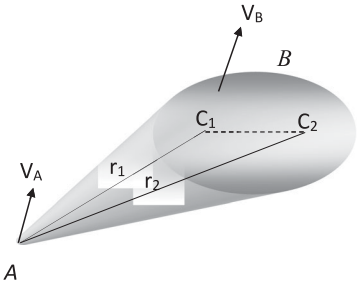

Fig. 3. A point and a hyperspheroid.

In the next sections, we demonstrate how these results can be used to determine analytical expressions for the collision cones between a point object and an n-dimensional hyperspheroid and a hyperboloid, moving in n-dimensional space.

III. Collision Cone Between a Point Object and a Hyperspheroid

Consider a point object A and a hyperspheroid B moving in n-dimensional space. Here, B is defined by the equation:

$$\frac{x_1^2}{a^2} + \frac{x_2^2 + x_3^2 + \ldots + x_n^2}{b^2} = 1 \tag{16}$$

and represents the surface generated by the locus of points such that the sum of distances from the foci of B is a constant equal to $2a$. When reduced to 2-dimensions, B is an ellipse, while in 3-dimensions, it is a spheroid.

Refer Fig. 3, which for easy visualization gives the hyperspheroid in 3-D, but the notations used carry through in n-dimensions. Let C_1 and C_2 represent the two foci of B. Let $V_{r,C1}$, $V_{\phi 1,C1}$, $V_{\phi 2,C1}$, …, $V_{\phi n-1,C1}$ represent the relative velocity components of C_1 with respect to A, and $V_{r,C2}$, $V_{\phi 1,C2}$, $V_{\phi 2,C2}$, …, $V_{\phi n-1,C2}$ represent the relative velocity components of C_2 with respect to A. Here, $V_{r,C1}$ (respectively, $V_{r,C2}$) represent the relative velocity component along AC_1 (respectively, AC_2). Let r_{m1} represent the distance between A and C_1 at the instant of closest approach, and r_{m2} represent the corresponding distance between A and C_2 at the instant of closest approach. Let the corresponding times, at which these closest approaches occur, be t_{m1} and t_{m2}, respectively. Then, from (14), we see that $r_{mi}, i = 1, 2$ is as follows:

$$r_{mi}^2 = \frac{r_i(0)^2(V_{\phi 1,Ci}(0)^2 + \ldots + V_{\phi n-1,Ci}(0)^2)}{V_{r,Ci}(0)^2 + V_{\phi 1,Ci}(0)^2 + \ldots + V_{\phi n-1,Ci}(0)^2} \tag{17}$$

and, from (15), $t_{mi}, i = 1, 2$ is as follows:

$$t_{mi} = \frac{-r_i(0)V_{r,Ci}(0)}{V_{r,Ci}(0)^2 + V_{\phi 1,Ci}(0)^2 + \ldots + V_{\phi n-1,Ci}(0)^2} \tag{18}$$

Consider (9), when applied individually to the lines AC_1 and AC_2. Using (7) in (9), we get the equation:

$$V_{r,Ci}^2 + r_i\dot{V}_{r,Ci} = V_{r,Ci}(0)^2 + V_{\phi 1,Ci}(0)^2 + \ldots + V_{\phi n-1,Ci}(0)^2, i = 1, 2 \tag{19}$$

When A and B move with constant velocities, the right hand side of (19) is the same for $i = 1, 2$, and we refer to this as V_C^2. Replacing $V_{r,Ci}^2$ by $V_{r,Ci}\dot{r}_i$ in the above equation, we obtain:

$$V_{r,Ci}\dot{r}_i + r_i\dot{V}_{r,Ci} = V_C^2,\ i = 1, 2 \tag{20}$$

Integrating the above equation for $i = 1$ from limits t_{m1} to t (where we assume, without loss of generality, that $t_{m1} < t < t_{m2}$), we get:

$$\int_{t_{m1}}^{t} d(r_1V_{r,C1}) = \int_{t_{m1}}^{t} V_C^2$$
$$\Rightarrow r_1V_{r,C1} - r_{m1}V_{rm1} = V_C^2(t - t_{m1}) \tag{21}$$

Since $V_{rm1} = 0$, therefore (21) becomes:

$$r_1\dot{r}_1 = V_C^2(t - t_{m1}) \tag{22}$$

Integrating (22), we get:

$$\int_{t_{m1}}^{t} r_1\dot{r}_1 = \int_{t_{m1}}^{t} V_C^2(t - t_{m1})$$
$$\Rightarrow r_1(t)^2 = r_{m1}^2 + V_C^2(t - t_{m1})^2 \tag{23}$$

Next, integrating (20) for $i = 2$ from limits t to t_{m2}, and following steps similar to (21)–(23), we get:

$$\Rightarrow r_2(t)^2 = r_{m2}^2 + V_C^2(t_{m2} - t)^2 \tag{24}$$

From (23), (24), we then get the following:

$$r_1 + r_2 = \sqrt{r_{m1}^2 + V_C^2(t - t_{m1})^2} + \sqrt{r_{m2}^2 + V_C^2(t_{m2} - t)^2} \tag{25}$$

Let t_m represent the time at which $r_1 + r_2$ is a minimum. This corresponds to the time instant when A and B are at their closest approach, and this can be found by differentiating (25) with respect to t and equating to zero. The equation $\frac{d(r_{C1}+r_{C2})}{dt} = 0$ yields the expression:

$$\frac{V_C^2(t - t_{m1})}{\sqrt{r_{m1}^2 + V_C^2(t - t_{m1})^2}} - \frac{V_C^2(t_{m2} - t)}{\sqrt{r_{m2}^2 + V_C^2(t_{m2} - t)^2}} = 0 \tag{26}$$

The above equation is solved for t_m as follows:

$$t_m = \frac{r_{m2}t_{m1} + r_{m1}t_{m2}}{r_{m1} + r_{m2}} \tag{27}$$

Substituting $t = t_m$ in (25), where t_m is obtained from (27), we can obtain r_m as follows:

$$r_m^2 = (V_r^2 + V_{\phi 1}^2 + \ldots + V_{\phi n-1}^2)(t_{m2} - t_{m1})^2 + (r_{m1} + r_{m2})^2 \tag{28}$$

Since collision occurs when $r_m \leq 2a$, therefore the collision condition between A and B is given by the following expression:

$$[r_1V_{r,C1} - r_2V_{r,C2}]^2 + \left[r_1\sqrt{V_{\phi 1,C1}^2 + \ldots + V_{\phi n-1,C1}^2} + r_2\sqrt{V_{\phi 1,C2}^2 + \ldots + V_{\phi n-1,C2}^2}\right]^2 \leq 4a^2V_C^2 \tag{29}$$

which is obtained after substituting r_{m1}, r_{m2} from (17) and t_{m1}, t_{m2} from (18) in (29). Additionally, since it is required that t_m

in (27) always satisfies $t_m \geq 0$ (that is, the collision condition is computed only for all future time), this means that:

$$V_{r,C2}\sqrt{V_{\phi 1,C1}^2 + V_{\phi 2,C1}^2 + \ldots + V_{\phi n-1,C1}^2} + V_{r,C1}\sqrt{V_{\phi 1,C2}^2 + V_{\phi 2,C2}^2 + \ldots + V_{\phi n-1,C2}^2} \leq 0 \quad (30)$$

Thus, if a point and a hyperspheroid are moving such that (29) and (30) are satisfied, then they are on a collision course with each other.

As a footnote, we observe that when B is a hypersphere of radius R, then the two foci merge into the center of B, in which case, $V_{r,C1} = V_{r,C2} \equiv V_r$, $V_{\phi j,C1} = V_{\phi j,C2} \equiv V_{\phi j}, j = 1, 2, \ldots, n-1$, $a = R$, and (29) and (30) collapse to the conditions:

$$r^2(V_{\phi 1}^2 + \ldots + V_{\phi n-1}^2) \leq R^2(V_r^2 + V_{\phi 1}^2 + \ldots + V_{\phi n-1}^2) \quad (31)$$

$$V_r < 0 \quad (32)$$

Considering (29) and (30), we define two scalar quantities y and $V_{r,AB}$ as follows:

$$y = [r_1 V_{r,C1} - r_2 V_{r,C2}]^2 + \left[r_1\sqrt{V_{\phi 1,C1}^2 + \ldots + V_{\phi n-1,C1}^2} + r_2\sqrt{V_{\phi 1,C2}^2 + \ldots + V_{\phi n-1,C2}^2}\right]^2 - 4a^2V_C^2 \quad (33)$$

$$V_{r,AB} = V_{r,C2}\sqrt{V_{\phi 1,C1}^2 + \ldots + V_{\phi n-1,C1}^2} + V_{r,C1}\sqrt{V_{\phi 1,C2}^2 + \ldots + V_{\phi n-1,C2}^2} \quad (34)$$

Here, y is essentially a miss-distance function such that, when $V_{R,AB} < 0$, then $y = 0$ corresponds to the scenario where A will graze the surface of B, $y < 0$ corresponds to the scenario where A will enter B, and $y > 0$ implies that A will pass around B. The equation $y = c$ (where c is a constant) represents a manifold in the $(r_{Ci}, V_{r,Ci}, V_{\phi 1,Ci}, V_{\phi 2,Ci}, V_{\phi 3,Ci}, \ldots, V_{\phi n-1,Ci})$ space. The collision cone $\mathcal{X}$ is then defined as follows:

$$\mathcal{X} = \{\alpha_1, \alpha_2, \ldots, \alpha_{n-1} : y \leq 0, V_{r,AB} < 0\} \quad (35)$$

and represents the instantaneous set of heading angles of A for which A is on a collision course with B.

IV. Collision Cone Between a Point Object and a Confocal Quadric

We next consider a hyperboloid in n-dimensions, which is represented by the following equation:

$$\frac{x_1^2}{a_h^2} - \frac{x_2^2 + x_3^2 + \ldots + x_n^2}{b_h^2} = 1 \quad (36)$$

Such a hyperboloid is a two-sheeted hyperboloid, and is characterized by the property that it is the locus of all points that satisfy the relation $|r_1 - r_2| \leq 2a_h$, where r_1 and r_2 represent the distances of a point on the hyperboloid to the two foci, and a_h represents the semi-major axis of the hyperboloid. The hyperboloid is non-convex, and of infinite extent.

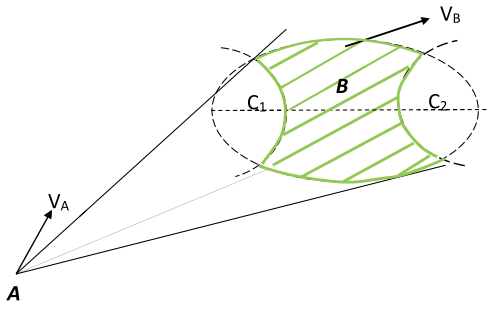

Fig. 4. A point and a non-convex confocal quadric.

However, the object B formed by the intersection of the n-dimensional hyperboloid with a n-dimensional hyperspheroid (with both objects sharing the same foci) is of finite extent, and non-convex, as is illustrated in Fig. 4. Such a confocal quadric can be used to approximate a class of non-convex shapes.

As before, let r_1 and r_2 represent the distances of the point object A to the two foci C_1 and C_2 of B. We note that in order for the point A to collide with B, it must first hit the associated hyperspheroid, since B is contained inside the hyperspheroid. Let t_m represent the time of closest approach of A to the hyperspheroid, as given in (27). The point A is on a collision course with B if $|r_1(t_m) - r_2(t_m)| \leq 2a_h$. Substituting r_1 and r_2 from (23), (24) and t_m from (27), this leads to the following condition:

$$\left[r_{C1}\sqrt{\sum_{j=1}^{n-1} V_{\phi j,C1}^2} - r_{C2}\sqrt{\sum_{j=1}^{n} V_{\phi j,C2}^2}\right]^2 + (r_{C2}V_{r,C2} - r_{C1}V_{r,C1})^2 \times \left[\frac{r_{C1}\sqrt{\sum_{j=1}^{n-1} V_{\phi j,C1}^2} - r_{C2}\sqrt{\sum_{j=1}^{n-1} V_{\phi j,C2}^2}}{r_{C1}\sqrt{\sum_{j=1}^{n} V_{\phi j,C1}^2} + r_{C2}\sqrt{\sum_{j=1}^{n-1} V_{\phi j,C2}^2}}\right]^2 \leq 4a_h^2V_C^2 \quad (37)$$

Accordingly, we define a scalar quantity y_h, which represents a miss-distance function from A to B as follows:

$$y_h = \left[r_{C1}\sqrt{\sum_{j=1}^{n-1} V_{\phi j,C1}^2} - r_{C2}\sqrt{\sum_{j=1}^{n} V_{\phi j,C2}^2}\right]^2 + (r_{C2}V_{r,C2} - r_{C1}V_{r,C1})^2 \times \left[\frac{r_{C1}\sqrt{\sum_{j=1}^{n-1} V_{\phi j,C1}^2} - r_{C2}\sqrt{\sum_{j=1}^{n-1} V_{\phi j,C2}^2}}{r_{C1}\sqrt{\sum_{j=1}^{n} V_{\phi j,C1}^2} + r_{C2}\sqrt{\sum_{j=1}^{n-1} V_{\phi j,C2}^2}}\right]^2 - 4a_h^2V_C^2 \quad (38)$$

The collision cone between A and B is then defined as:

$$\mathcal{X} = \{\alpha_1, \alpha_2, \ldots, \alpha_{n-1} : y \leq 0, V_{r,AB} < 0, y_h \leq 0\} \quad (39)$$

and represents the set of heading angles of A for which A is on a collision course with B.

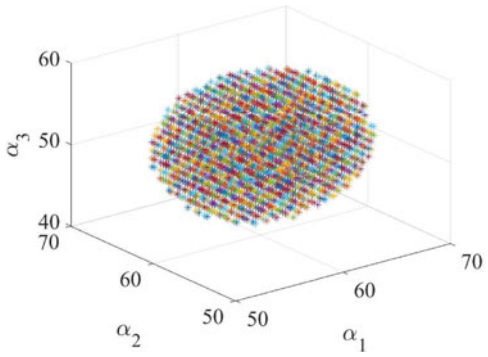

Fig. 5. Example illustrating the collision cone in a 4-D space.

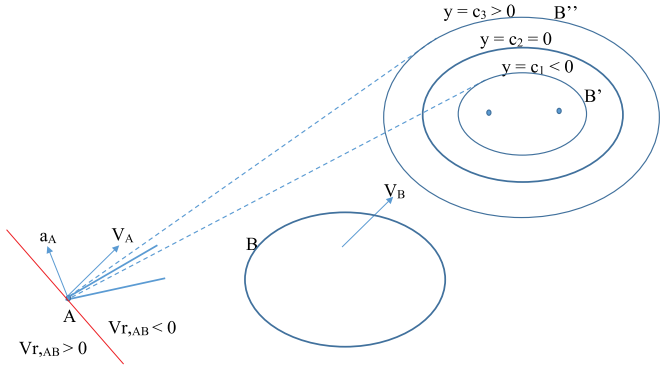

Fig. 6. Illustration of level sets corresponding to hyperspheroid B.

V. Example

We now illustrate the utility of the collision cone concept with an example. Consider a point object A and a hyperspheroid B moving in a 4-dimensional space. At some time t_k, the position of A is $(-10, -15, -20, -25)$, while the position of the foci C_1 and C_2 of the hyperspheroid B are $(5, 0, 0, 0)$ and $(-5, 0, 0, 0)$, respectively. The semi-major axis of the hyperspheroid is taken as $a = 7$. A is moving with speed $V_A = 7\,\mathrm{m/sec}$, while B has a speed $V_B = 2\,\mathrm{m/sec}$. The heading angles of $\vec{V}_B$ are defined by $(\beta_1, \beta_2, \beta_3) = (20^0, 25^0, 35^0)$. Using (33)–(35), Fig. 5 shows the point cloud comprising the instantaneous set of heading angles $(\alpha_1, \alpha_2, \alpha_3)$ that will cause A to be on a collision course with B. If B continues to move with constant velocity, and A has its velocity vector anywhere inside this point cloud, then it is guaranteed that A will collide with B. We note that for each heading direction that lies in the point cloud, an approximate time to collision can be determined.

The point cloud can be integrated with an RRT algorithm as follows. If the hyperspheroid B represents an obstacle, then the RRT algorithm may choose the heading for the next waypoint for A such that it avoids the point cloud altogether. At a second level, the RRT algorithm may assign a time-to-collision threshold, based on which it could ignore points in the point cloud for which the time-to-collision lies above this threshold. It could then consider the subsequent reduced-size point cloud and choose the heading for the next waypoint such that it avoids this reduced-size point cloud.

On the other hand, if the hyperspheroid B represents an area wherein the trajectory of A should lie, then the RRT algorithm may choose the heading for the next waypoint such that it lies in the point cloud, or at least lies in the point cloud with a higher probability.

VI. Path Planning

The scalar quantities y defined in (33) (or y_h defined in (38)) can be used to provide a foundation for path planning in n-dimensional spaces. They have the property that when A and B move at constant velocities, $y = \text{constant}$ ($y_h = \text{constant}$), a fact that is readily demonstrated by verifying that $dy/dt = 0$ ($dy_h/dt = 0$) when evaluated along the system trajectories. Furthermore, the equations $y = c$ and $y_h = c$, where c is a constant, can be viewed as level sets. Level sets with $y = c > 0$ correspond to "virtual" hyperspheroids that contain the original hyperspheroid B, while level sets with $y = c < 0$ correspond to virtual hyperspheroids that lie inside B. By applying an acceleration a_A, the "aiming point" of the velocity vector of A can be shifted from one level set to another. Thus, when A has the objective of avoiding a collision with B, a_A may be applied to modify the relative velocity vector such that y changes from a negative value to a non-negative one. On the other hand, when A has the objective of performing a rendezvous with B, then a_A may be applied to drive the relative velocity vector into the $y < 0$, $V_{r,AB} < 0$ region.

This is schematically illustrated in Fig. 6. The position of A and the hyperspheroid B at time $t = 0$ are shown. Also shown is the position of B at time $t = t_m$, and two representative level sets of B, represented as B' and B'', that are confocal with B and lie inside and outside B, respectively, at $t = t_m$. The level set corresponding to B is associated with $y = 0$. In order for A to graze the boundary of this level set, the velocity vector $\vec{V}_A$ needs to be aligned with the boundary of the collision cone $\mathcal{X}$. The level sets corresponding to B' and B'' are associated with $y = c_1 < 0$ and $y = c_2 > 0$, respectively, and for A to graze the boundary of either of these level sets, the velocity vector of A needs to be as shown in the figure.

The acceleration vector of A is represented by its components in n-dimensions as:

$$\vec{a}_A = a_A \begin{bmatrix} \cos\gamma_1 \\ \sin\gamma_1 \cos\gamma_2 \\ \sin\gamma_1 \sin\gamma_2 \cos\gamma_3 \\ \vdots \\ \sin\gamma_1 \sin\gamma_2 \ldots \sin\gamma_{n-2} \cos\gamma_{n-1} \\ \sin\gamma_1 \sin\gamma_2 \ldots \sin\gamma_{n-2} \sin\gamma_{n-1} \end{bmatrix}$$

where, $\gamma_1, \gamma_2, \ldots, \gamma_{n-1}$ represent the angles associated with $\vec{a}_A$. Then, when A has a non-zero acceleration, the kinematic differential equations governing the relative velocity of B with

respect to A are as follows:

$$\begin{bmatrix} \dot{r}_i \\ \dot{\phi}_{1,Ci} \\ \dot{\phi}_{2,Ci} \\ \vdots \\ \dot{\phi}_{n-1,Ci} \\ \dot{V}_{r,Ci} \\ \dot{V}_{\phi 1,Ci} \\ \vdots \\ \dot{V}_{\phi n-1,Ci} \end{bmatrix} = \begin{bmatrix} V_{r,Ci} \\ \frac{V_{\phi 1,Ci}}{r_i} \\ \frac{V_{\phi 2,Ci}}{r_i \sin\phi_{1,Ci}} \\ \vdots \\ \frac{V_{\phi n-1,Ci}}{r_i \sin\phi_{1,Ci} \sin\phi_{2,Ci} \ldots \sin\phi_{n-2,Ci}} \\ \frac{V_{\phi 1,Ci}^2 + V_{\phi 2,Ci}^2 + V_{\phi 3,Ci}^2}{r_i} \\ \cdots \\ \cdots \\ \cdots \end{bmatrix} + \begin{bmatrix} 0 \\ 0 \\ 0 \\ \vdots \\ 0 \\ -\hat{a}_A.\hat{\epsilon}_{r,Ci} \\ -\hat{a}_A.\hat{\epsilon}_{\phi 1,Ci} \\ \cdots \\ -\hat{a}_A.\hat{\epsilon}_{\phi n-1,Ci} \end{bmatrix} a_A, \; i = 1, 2 \tag{40}$$

where, $\hat{a}_A$ represents the unit acceleration vector of A. Equation (40) is given for a 4-D scenario in the Appendix.

We now determine a guidance law for a_A that will enable $\vec{V}_A$ to change its aiming point from its current level set to another level set. Toward this end, define a Lyapunov function:

$$L = \frac{1}{2}(y - w)^2 \tag{41}$$

where, w corresponds to the level set that needs to be attained. We then determine an acceleration magnitude a_A that will make $\dot{L}$ negative definite, and this is a necessary condition to ensure that the level set corresponding to $y = w$ is attained. Since $\dot{L} = (y - w)(\dot{y} - \dot{w})$, where $\dot{y}$ is given by:

$$\begin{aligned} \frac{dy}{dt} = \sum_{i=1}^{2} \Bigg[& \frac{\partial y}{\partial r_i} V_{r,Ci} \\ & + \frac{\partial y}{\partial \phi_{1,Ci}} \dot{\phi}_{1,Ci} + \ldots + \frac{\partial y}{\partial \phi_{n-1,Ci}} \dot{\phi}_{n-1,Ci} \\ & + \frac{\partial y}{\partial V_{\phi 1,Ci}} \dot{V}_{\phi 1,Ci} + \ldots + \frac{\partial y}{\partial V_{\phi n-1,Ci}} \dot{V}_{\phi n-1,Ci} \\ & + \frac{\partial y}{\partial V_{r,Ci}} \dot{V}_{r,Ci} \Bigg] \end{aligned} \tag{42}$$

It can then be seen that if we choose:

$$a_A = \frac{K/2(y - w)}{D} \tag{43}$$

where,

$$\begin{aligned} D = \sum_{i=1}^{2} \Bigg[& \frac{\partial y}{\partial V_{\phi 1,Ci}} (\hat{a}_A.\hat{\epsilon}_{\phi 1,Ci}) + \ldots \\ & + \frac{\partial y}{\partial V_{\phi n-1,Ci}} (\hat{a}_A.\hat{\epsilon}_{\phi n-1,Ci}) + \frac{\partial y}{\partial V_{r,Ci}} (\hat{a}_A.\hat{\epsilon}_{r,Ci}) \Bigg] \end{aligned} \tag{44}$$

then this will make the Lyapunov equation follow the dynamics $\dot{L} = -KL$. Assuming $V_{r,AB} < 0$, we require that $K > 0$ for $\dot{L}$ to be negative definite. Furthermore, since the Lyapunov function follows the dynamics $L(t) = L(0)e^{-Kt}$, we need that $K > \frac{1}{t_m} \ln \frac{L(0)}{\epsilon}$ (where $\epsilon < L(0)$) in order to ensure that L decays to ϵ (that is, the aiming point of $\vec{V}_A$ comes within $\sqrt{\epsilon}$ of the $y = w$ level set by the time t_m given in (27)).

VII. Conclusion

In this letter, analytical expressions of collision cones associated with a class of hyperquadric surfaces moving in n-dimensional configuration spaces, are determined. The collision cone provides the set of instantaneous heading angles of an object in n-dimensional space that will cause it to be on a collision course with another object. Analytical expressions of the collision cone are immensely helpful because of the computational savings they can provide. For instance, when used in conjunction with sampling-based planners such as RRTs and PRMs, the motion planners need not evaluate sample waypoints that lie inside a collision cone, or they may evaluate them with low probability. The cones can also be constructed to lead to desirable regions of the configuration space, in which case, the motion planners may evaluate samples that lie inside the cone, with higher probability.

Analytical expressions of these cones also serve as an efficient platform for the design of acceleration laws that enable an object to drive its velocity vector out of the collision cone (when the application is one of collision avoidance), or alternatively, drive its velocity vector into the cone (when the application is one of capturing a target, or of entering a desired region in the configuration space). A Lyapunov-based approach is used to determine such a nonlinear guidance law, that can effectively change the heading of the velocity vector of the object, as desired.

Appendix
Illustrative 4-D Example

In a 4-D scenario, after writing the full form expressions of each of the four relative velocity components, differentiating the resulting expressions, and re-arranging the algebraic terms, we obtain the following four differential equations:

$$\begin{aligned} \dot{V}_r &= \dot{\phi}_1 V_{\phi 1} + \sin\phi_1 \dot{\phi}_2 V_{\phi 2} + \sin\phi_1 \sin\phi_2 \dot{\phi}_3 V_{\phi 3} \\ \dot{V}_{\phi 1} &= -\dot{\phi}_1 V_r + \cos\phi_1 \dot{\phi}_2 V_{\phi 2} + \cos\phi_1 \sin\phi_2 \dot{\phi}_3 V_{\phi 3} \\ \dot{V}_{\phi 2} &= \dot{\phi}_2(-V_{\phi 1} \cos\phi_1 - V_r \sin\phi_1) + \cos\phi_2 \dot{\phi}_3 V_{\phi 3} \\ \dot{V}_{\phi 3} &= -\dot{\phi}_3(V_{\phi 2} \cos\phi_2 + V_{\phi 1} \cos\phi_1 \sin\phi_2 + V_r \sin\phi_1 \sin\phi_2) \end{aligned} \tag{45}$$

Equation (45) thus represent the differential equations governing the kinematics of the engagement between A and B in 4-D space. By eliminating $\dot{\phi}_1$, $\dot{\phi}_2$, and $\dot{\phi}_3$ from these equations, after some rearrangement of the terms, we eventually get the following:

$$r\dot{V}_r = V_{\phi 1}^2 + V_{\phi 2}^2 + V_{\phi 3}^2 \tag{46}$$

$$r\dot{V}_{\phi 1} = -V_{\phi 1}V_r + \cot\phi_1(V_{\phi 2}^2 + V_{\phi 3}^2) \tag{47}$$

$$r\dot{V}_{\phi 2} = -V_{\phi 1}V_{\phi 2}\cot\phi_1 - V_{\phi 2}V_r + \cot\phi_2 \operatorname{cosec}\phi_1 V_{\phi 3}^2 \tag{48}$$

$$r\dot{V}_{\phi 3} = -V_{\phi 2}V_{\phi 3}\operatorname{cosec}\phi_1\cot\phi_2 - V_{\phi 1}V_{\phi 3}\cot\phi_1 - V_{\phi 3}V_r \tag{49}$$

Multiplying (46)–(49) by $V_r, V_{\phi 1}, V_{\phi 2}, V_{\phi 3}$, respectively, and adding the resulting equations, we obtain:

$$\dot{V}_r V_r + \dot{V}_{\phi 1}V_{\phi 1} + \dot{V}_{\phi 2}V_{\phi 2} + \dot{V}_{\phi 3}V_{\phi 3} = 0 \tag{50}$$

which can be integrated to yield:

$$V_r^2 + V_{\phi 1}^2 + V_{\phi 2}^2 + V_{\phi 3}^2 = V_r^2(0) + V_{\phi 1}^2(0) + V_{\phi 2}^2(0) + V_{\phi 3}^2(0) \tag{51}$$

where, $V_r(0), V_{\phi 1}(0), V_{\phi 2}(0), V_{\phi 3}(0)$ represent the initial values of the corresponding quantities.

Furthermore, by multiplying (47)–(49) by $V_{\phi 1}$, $V_{\phi 2}$, and $V_{\phi 3}$, respectively, and adding the resulting terms, we obtain the equation:

$$\frac{\dot{V}_{\phi 1}V_{\phi 1} + \dot{V}_{\phi 2}V_{\phi 2} + \dot{V}_{\phi 3}V_{\phi 3}}{V_{\phi 1}^2 + V_{\phi 2}^2 + V_{\phi 3}^2} = \frac{-V_r}{r} \tag{52}$$

The illustration for (40), involving the kinematic equations governing the relative velocity of B with respect to A, in 4-dimensional space are as given below:

$$\begin{bmatrix} \dot{r}_i \\ \dot{\phi}_{1,Ci} \\ \dot{\phi}_{2,Ci} \\ \dot{\phi}_{3,Ci} \\ \dot{V}_{\phi 1,Ci} \\ \dot{V}_{\phi 2,Ci} \\ \dot{V}_{\phi 3,Ci} \\ \dot{V}_{r,Ci} \end{bmatrix} = \begin{bmatrix} V_{r,Ci} \\ V_{\phi 1,Ci}/r_i \\ P \\ Q \\ R/r_i \\ S/r_i \\ T/r_i \\ U/r_i \end{bmatrix} + \begin{bmatrix} 0 \\ 0 \\ 0 \\ 0 \\ -\hat{a}_A.\hat{\epsilon}_{\phi 1,Ci} \\ -\hat{a}_A.\hat{\epsilon}_{\phi 2,Ci} \\ -\hat{a}_A.\hat{\epsilon}_{\phi 3,Ci} \\ -\hat{a}_A.\hat{\epsilon}_{r,Ci} \end{bmatrix} a_A, \ i = 1, 2 \tag{53}$$

where,

$$\begin{aligned} P &= V_{\phi 2,Ci}/(r_i \sin\phi_{1,Ci}) \\ Q &= V_{\phi 3,Ci}/(r_i \sin\phi_{1,Ci} \sin\phi_{2,Ci}) \\ R &= -V_{\phi 1,Ci}V_{r,Ci} + \cot\phi_{1,Ci}(V_{\phi 2,Ci}^2 + V_{\phi 3,Ci}^2) \\ S &= -V_{\phi 1,Ci}V_{\phi 2,Ci}\cot\phi_{1,Ci} - V_{\phi 2,Ci}V_{r,Ci} \\ &\quad + \cot\phi_{2,Ci}\operatorname{cosec}\phi_{1,Ci}V_{\phi 3,Ci}^2 \\ T &= -V_{\phi 2,Ci}V_{\phi 3,Ci}\operatorname{cosec}\phi_{1,Ci}\cot\phi_{2,Ci} \\ &\quad - V_{\phi 1,Ci}V_{\phi 3,Ci}\cot\phi_{1,Ci} - V_{\phi 3,Ci}V_{r,Ci} \\ U &= V_{\phi 1,Ci}^2 + V_{\phi 2,Ci}^2 + V_{\phi 3,Ci}^2 \end{aligned} \tag{54}$$

REFERENCES

[1] Y. Yan, Q. Ma, and G. S. Chirikjian, "Path planning based on closed-form characterization of collision-free configuration-spaces for ellipsoidal bodies, obstacles, and environments," in *Proc. 1st Int. Workshop Robot Learn. Planning*, Ann Arbor, MI, USA, Jun. 18, 2016, pp. 13–19.

[2] D. Xing, F. Liu, S. Liu, and D. Xu, "Motion control for cylindrical objects in microscopes view using a projection method I: Collision detection and detach control," *IEEE Trans. Ind. Electron.*, vol. 64, no. 7, pp. 5524–5533, Jul. 2017.

[3] L. E. Kavraki, P. Svestka, J.-C Latombe, and M. H. Overmars, "Probabilistic roadmaps for path planning in high-dimensional configuration spaces," *IEEE Trans. Robot. Autom.*, vol. 12, no. 4, pp. 566–580, Aug. 1996.

[4] S. M. LaValle and J. J. Kuffner, "Randomized kinodynamic planning," *Int. J. Robot. Res.*, vol. 20, no. 5, 2001, Art. no. 378400.

[5] Y. Yan and G. S. Chirikjian, "Closed-form characterization of the Minkowski sum and difference of two ellipsoids," *Geom Dedicata*, vol. 77, pp. 103–128, 2015.

[6] Q. Ma and G. S. Chirikjian, "A closed-form lower bound on the allowable motion for an ellipsoidal body and environment," in *Proc. ASME 2015 Int. Design Eng. Tech. Conf. Comput. Inform. Eng. Conf.*, (Volume 5C: 39th Mechanisms and Robotics Conference, Boston, MA, USA), Aug. 2–5, 2015, pp. V05CT08A055, 10 pages.

[7] A. Chakravarthy and D. Ghose, "Obstacle avoidance in a dynamic environment: A collision cone approach," *IEEE Trans. Syst., Man, Cybern., Part A Syst. Humans*, vol. 28, no. 5, pp. 562–574, Sep. 1998.

[8] A. J. Hanson, "Hyperquadrics: Smoothly deformable shapes with convex polyhedral bounds," *Comput. Vis., Graph., Image Process.*, vol. 44, no. 2, pp. 191–210, Nov. 1988,

[9] J. D. Gammell, S. S. Srinivasa, and T. D. Barfoot, "Informed RRT*: Optimal sampling-based path planning focused via direct sampling of an admissible ellipsoidal heuristic," in *Proc. IEEE/RSJ Int. Conf. Intell. Robots Sys.*, 2014, pp. 2997–3004.

[10] A. Chakravarthy and D. Ghose, "Collision cones for quadric surfaces," *IEEE Trans. Robot.*, vol. 27, no. 6, pp. 1159–1166, Dec. 2011.

[11] A. Chakravarthy and D. Ghose, "Generalization of the collision cone approach for motion safety in 3-dimensional environments," *Auton. Robots*, vol. 32, no. 3, pp. 243–266, Apr. 2012.

[12] A. Chakravarthy and D. Ghose, "Guidance laws for precision 3-dimensional maneuvers through orifices using safe-passage cones," *J. Guid., Control Dyn.*, vol. 39, no. 6, pp. 1325–1341, 2016.

[13] L. P. Tychonievich, D. Zaret, R. Mantegna, R. Evans, E. Muehle, and S. Martin, "A maneuvering-board approach to path planning with moving obstacles," in *Proc. Int. Joint Conf. Artif. Intell.*, 1989, pp. 1017–1021.

[14] P. Fiorini and Z. Shiller, "Motion planning in dynamic environments using velocity obstacles," *Int. J. Robot. Res.*, Oxford Univ. Press, vol. 17, no. 7, pp. 760–772, 1998.

[15] B. Damas and J. Santos-Victor, "Avoiding moving obstacles: the forbidden velocity map," in *Proc. IEEE/RSJ Int. Conf. Intell. Robots Syst.*, 2009, pp. 4393–4398.

[16] J. R. Weeks, *The Shape of Space*, Boca Raton, FL, USA: CRC Press, 2001.

[17] C. S. Carlson, "A Study of the Hyperquadrics in Euclidean space of four dimensions," M.S Thesis, State University of Iowa, Iowa City, IA, USA, 1928.